Transmission grating based extreme ultraviolet imaging spectrometer for time and space resolved impurity measurements[a)]

Deepak Kumar,[1,b)] Dan Stutman,[1] Kevin Tritz,[1] Michael Finkenthal,[1] Charles Tarrio,[2] and Steven Grantham[2]
[1]*Department of Physics and Astronomy, The Johns Hopkins University, Baltimore, Maryland 21218, USA*
[2]*Physics Laboratory, National Institute of Standards and Technology, Gaithersburg, Maryland 20899, USA*

(Presented 20 May 2010; received 17 May 2010; accepted 11 June 2010; published online 5 October 2010)

A free standing transmission grating based imaging spectrometer in the extreme ultraviolet range has been developed for the National Spherical Torus Experiment (NSTX). The spectrometer operates in a survey mode covering the approximate spectral range from 30 to 700 Å and has a resolving capability of $\delta\lambda/\lambda$ on the order of 3%. Initial results from space resolved impurity measurements from NSTX are described in this paper. © *2010 American Institute of Physics.* [doi:10.1063/1.3474661]

I. INTRODUCTION

Extreme ultraviolet (EUV) spectrometers for magnetic fusion experiments have traditionally employed grazing incidence gratings as the dispersive element. However, over the past decade, free standing transmission gratings have emerged as an excellent alternative to grazing incidence gratings for building survey spectrometers in the EUV range.[1–3] Not only do transmission gratings have the advantage of having higher diffraction efficiency and being robust to neutron exposure, but they also lead to a simplified design of the spectrometer.

The paper is structured as follows: Section II describes the design, calibration, and setup of a transmission grating based imaging spectrometer (TGIS). Setup of the TGIS on National Spherical Torus Experiment (NSTX) is described in Sec. III. The section also describes initial results from impurity identification and their spatial dependence.

II. DEVICE SETUP

Figure 1 describes the optical layout of the TGIS. The TGIS uses a Ta/SiC grating manufactured by NTT-ATT [part number ATN/TG-200/11W[4]]. The freestanding transmission grating has 5000 line-pairs/mm and dimensions 1×1 mm^2. The detector is an assembly of CsI coated microchannel plate (MCP), followed by a fiber optic phosphor screen with P20 phosphor (part number APD 3040FM 12/10/8, manufactured by Burle Industries, Inc., Lancaster, PA[4]). The rear end of the phosphor screen was fiber optically coupled to a CMOS based imaging sensor Radeye 1 manufactured by Rad-Icon Imaging Corp., Sunnyvale, CA.[4] The imaging system has a pixel size of 48 μm. While the imaging system has a resolution of 1024×512 pixels, only an area of approximately 400×400 pixels is covered by the spectrum. The frame rate for the line scan imaging system was 380 ms. The device has an angular view of 22° with a 1° resolution. A knife edge (perpendicular to the planar section shown in Fig. 1) is placed between the grating and the MCP to block half of the output spectrum including the zero order radiation.

A. Efficiency calibration

The transmission efficiency of a grating with an identical part number was calibrated at the Synchrotron Ultraviolet Radiation Facility at the National Institute of Standards and Technology (NIST). The setup for the calibration has been described by McMullin *et al.*[5] Figure 2 shows that the diffraction efficiencies in the range 115–304 Å (1 Å=0.1 nm) is relatively uniform around 0.1. For the calibrations, the polarization of the incident beam was oriented along the wires of the grating. The measured values have a relative uncertainty of 10%, which is dominated by the uncertainty in the geometry of the normalization of the measurements.

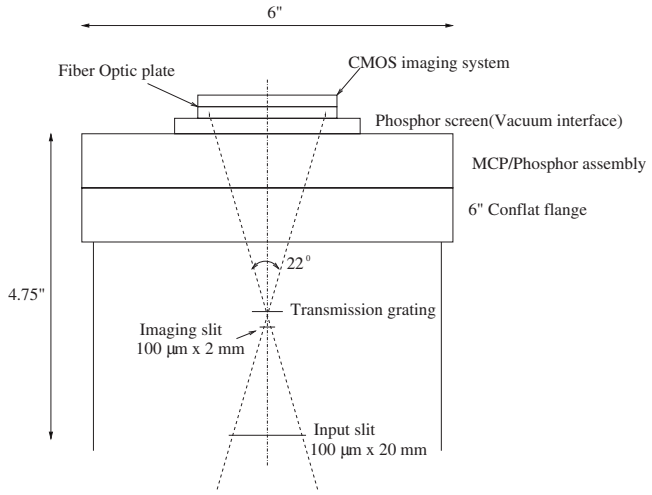

FIG. 1. Optical layout of the TGIS.

[a)]Contributed paper, published as part of the Proceedings of the 18th Topical Conference on High-Temperature Plasma Diagnostics, Wildwood, New Jersey, May 2010.
[b)]Electronic mail: deepak@pha.jhu.edu.

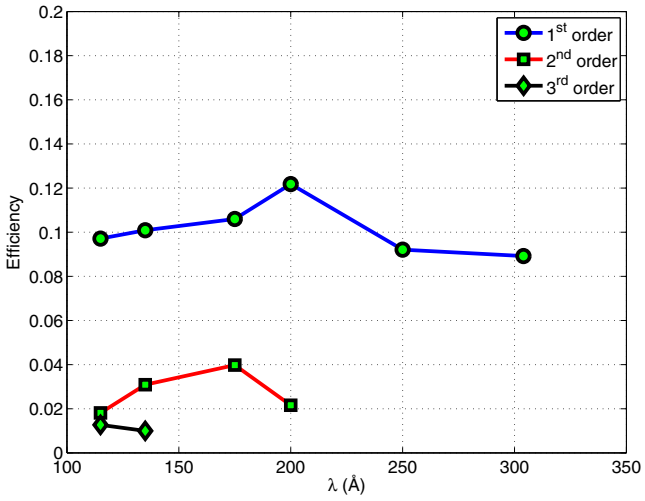

FIG. 2. (Color online) Diffraction efficiencies of the transmission grating.

B. Wavelength calibration

A table top reflex discharge was setup for wavelength and spatial calibration of the TGIS. The reflex discharge uses a cylindrical brass anode. Two circular Al cathodes are mounted close to the ends of the anode. A magnetic field of about 0.1 T links the cathodes. The reflex discharge was maintained within a 3–5 mTorr (1 Torr=133 Pa) pressure of Ne. Plasma was created by a dc discharge of approximately 1 kV applied across the electrodes with about 1 A current flowing through it. The TGIS measured the spectra through a rectangular opening on the brass anode. Figure 3 shows such a sample spectrum. Note that the spectrum extends from 24 to about 750 Å. Spectral features at 24 Å and the Al IV 161 Å lines indicate the presence of fast electrons in the reflex discharge and is being investigated further.

III. NSTX RESULTS

Figure 4 describes the view of the TGIS with respect to the heating neutral beam injection on NSTX.[6] Thus, the instrument measures the electron excited emission from the edge and the core and also the charge exchange radiation from the region of interaction with the beams.

Figure 5 shows the spectrum obtained from the TGIS on

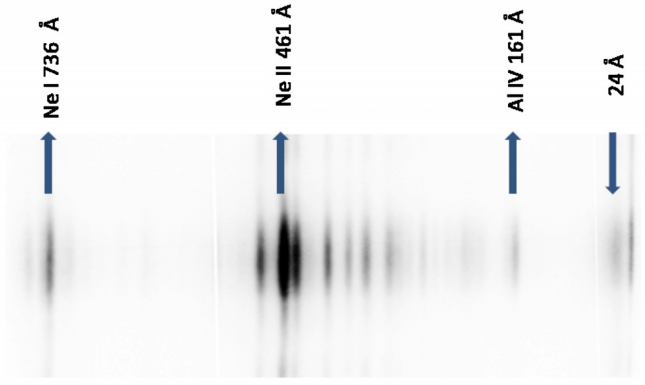

FIG. 3. (Color online) Spectrum from the reflex discharge used for wavelength calibration of the TGIS. Lines identified with the arrows pointing upward were used for the calibration.

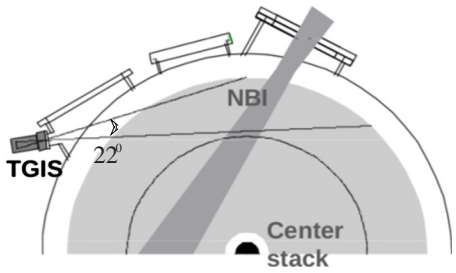

FIG. 4. (Color online) Midplane section of NSTX showing the orientation of TGIS with respect to the neutral beam on NSTX.

a typical neutral beam heated shot. In this particular experimental shot, the core electron temperature T_e was in the range of 0.8–1 keV and core electron density n_e was approximately 6×10^{19} m^{-3}. The charge exchange lines from C, O, and possibly Li are fairly well localized as indicated by the neutral beam interaction region bounded by the red dotted lines. This interaction region is located toward the periphery of the plasma. On the contrary, the emission from the three Cl lines is from a wide spatial region indicating that Li I and Be I like charge states of Cl are distributed closer to the core. Figure 6 shows the spectrum obtained by taking a "slice" along the vertical green arrow shown in Fig. 5.

In contrast to Fig. 5, the spectrum obtained from an Ohmic discharge at NSTX is shown in Fig. 7. In this particular experimental shot, the core electron temperature T_e was in the range of 0.6–1 keV and core electron density n_e was approximately 2×10^{19} m^{-3}. However, because of the absence of heating from neutral beam, the spectrum consists only of edge emission from low Z impurities.

It is instructive to consider the spatial distribution of certain representative lines. The spatial distribution of the impurities from the Ohmic spectrum is plotted in Fig. 8. Since the core electron temperature is between 0.6 and 1 keV, the emission is from the edge and highlights the spatial dependence of the edge impurities. However, the spatial dependence of the edge impurities in Fig. 8 is in stark contrast to the spatial profiles from a neutral beam heated shot

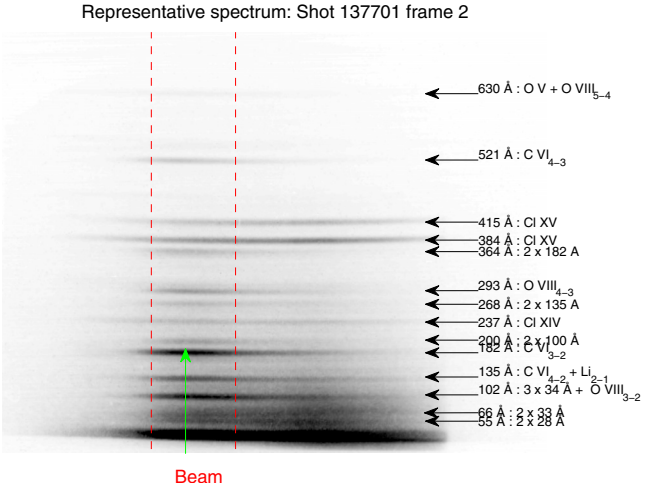

FIG. 5. (Color online) Typical spectrum obtained from neutral beam heated shot on NSTX. The transitions of the charge exchange line are shown in subscripts.

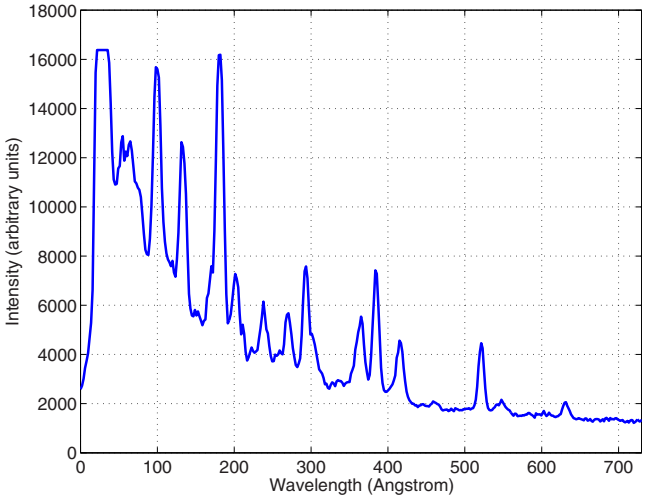

FIG. 6. (Color online) Spectrum obtained by taking a slice along the vertical green arrow shown in Fig. 5.

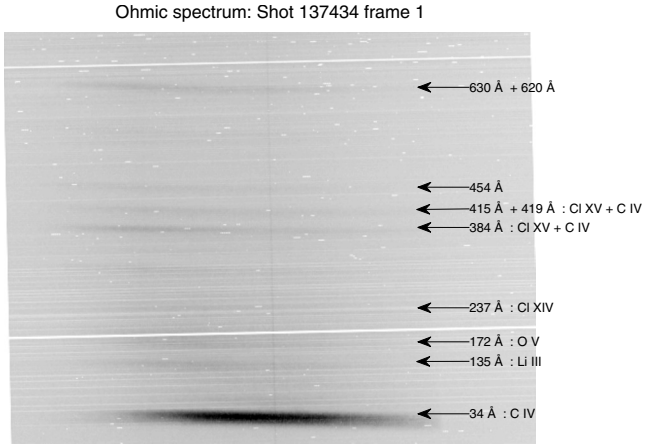

FIG. 7. Spectrum obtained from an Ohmic discharge on NSTX. Emission from C, O, and Li is expected to be from the edge.

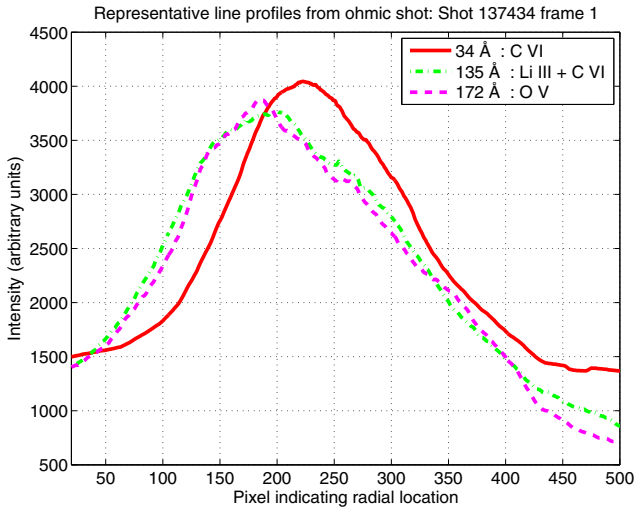

FIG. 8. (Color online) Spatial dependence of the edge emission from the Ohmic spectrum shown in Fig. 7. Note that the intensities of individual lines have been scaled for better comparison.

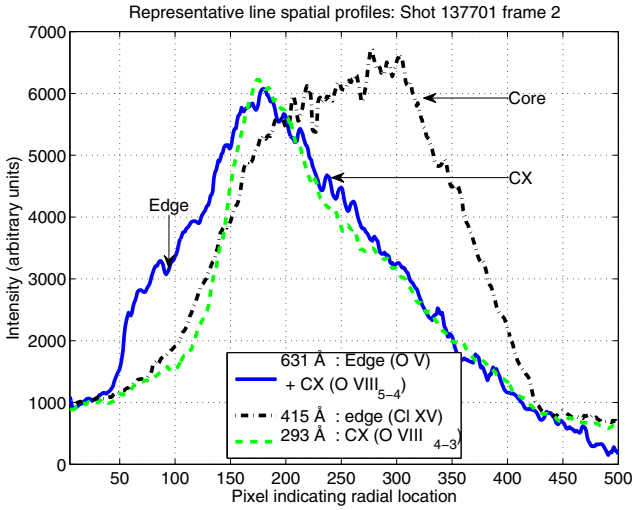

FIG. 9. (Color online) Spatial dependence of line intensity from Fig. 5 indicating the difference in charge exchange, edge, and core emission. Note that the intensities of individual lines have been scaled for better comparison.

shown in Fig. 9. In the figure, the profile of the Cl XV (415 Å) line is fairly broad, which is consistent with the fact that it is emitted from the core. The oxygen charge exchange lines shown in Fig. 9 have similar profiles (localized in the beam interaction region) except for some edge contribution from O V as highlighted in the figure.

IV. CONCLUSION

The results from Sec. III highlight the capability of space resolved impurity measurement by the TGIS. However, to gain more quantitative results on radial impurity distribution, a geometric model will be developed.

To enable monitoring of the time dependence of the impurity behavior, a faster readout imaging sensor is also being considered.

This paper highlights the use of the transmission grating for the EUV range. However, the instrument can be adapted to cover the vacuum ultraviolet (VUV) range as well by using a grating with 1000 line-pairs/mm. Such a VUV spectrometer has been tested on a tabletop experiment.

ACKNOWLEDGMENTS

The authors would like to thank Bryan Gaither (JHU) and the NSTX Team for their support. The work is supported by U.S. DOE Grant Nos. DE-S0000787, DE-FGO2-86ER53214, and DE-AC02-09CH11466.

[1] W. Wilhein, S. Rehbein, D. Hambach, M. Berglund, L. Rymell, and H. M. Hertz, Rev. Sci. Instrum. **70**, 1694 (1999).
[2] B. Blagojević, D. Stutman, M. Finkenthal, H. Moos, R. Kaita, and R. Majeski, Rev. Sci. Instrum. **74**, 1988 (2003).
[3] D. Stutman, G. Caravelli, M. Finkenthal, G. Wright, D. Whyte, N. Moldovan, R. Kaita, and L. Roquemore, J. Appl. Phys. **103**, 093307 (2008).
[4] Commercial products are mentioned only for experimental clarity. Any mention of commercial products does not constitute endorsement by the authors or the U.S. Government.
[5] D. McMullin, D. L. Judge, C. Tarrio, R. E. Vest, and F. Hanser, Appl. Opt. **43**, 3797 (2004).
[6] J. E. Menard, M. G. Bell, R. E. Bell, S. Bernabei, J. Bialek, T. Biewer, W. Blanchard, J. Boedo, C. E. Bush, M. D. Carter, W. Choe, N. A. Crocker,

D. S. Darrow, W. Davis, L. Delgado-Aparicio, S. Diem, C. W. Domier, D. A. D'Ippolito, J. Ferron, A. Field, J. Foley, E. D. Fredrickson, D. A. Gates, T. Gibney, R. Harvey, R. E. Hatcher, W. Heidbrink, K. W. Hill, J. C. Hosea, T. R. Jarboe, D. W. Johnson, R. Kaita, S. M. Kaye, C. E. Kessel, S. Kubota, H. W. Kugel, J. Lawson, B. P. LeBlanc, K. C. Lee, F. M. Levinton, N. C. Luhmann, Jr., R. Maingi, R. P. Majeski, J. Manickam, D. K. Mansfield, R. Maqueda, R. Marsala, D. Mastrovito, T. K. Mau, E. Mazzucato, S. S. Medley, H. Meyer, D. R. Mikkelsen, D. Mueller, T. Munsat, J. R. Myra, B. A. Nelson, C. Neumeyer, N. Nishino, M. Ono, H. K. Park, W. Park, S. F. Paul, T. Peebles, M. Peng, C. Phillips, A. Pigarov, R. Pinsker, A. Ram, S. Ramakrishnan, R. Raman, D. Rasmussen, M. Redi, M. Rensink, G. Rewoldt, J. Robinson, P. Roney, A. L. Roquemore, E. Ruskov, P. Ryan, S. A. Sabbagh, H. Schneider, C. H. Skinner, D. R. Smith, A. Sontag, V. Soukhanovskii, T. Stevenson, D. Stotler, B. C. Stratton, D. Stutman, D. Swain, E. Synakowski, Y. Takase, G. Taylor, K. Tritz, A. von Halle, M. Wade, R. White, J. Wilgen, M. Williams, J. R. Wilson, H. Yuh, L. E. Zakharov, W. Zhu, S. J. Zweben, R. Akers, P. Beiersdorfer, R. Betti, T. Bigelow, M. Bitter, P. Bonoli, C. Bourdelle, C. S. Chang, J. Chrzanowski, L. Dudek, P. C. Efthimion, M. Finkenthal, E. Fredd, G. Y. Fu, A. Glasser, R. J. Goldston, N. L. Greenough, L. R. Grisham, N. Gorelenkov, L. Guazzotto, R. J. Hawryluk, J. Hogan, W. Houlberg, D. Humphreys, F. Jaeger, M. Kalish, S. Krasheninnikov, L. L. Lao, J. Lawrence, J. Leuer, D. Liu, G. Oliaro, D. Pacella, R. Parsells, M. Schaffer, I. Semenov, K. C. Shaing, M. A. Shapiro, K. Shinohara, P. Sichta, X. Tang, R. Vero, M. Walker, and W. Wampler, Nucl. Fusion **47**, S645 (2007).